

# ANISOTROPIC TENSILE BEHAVIOUR OF UHPFRC: MESO-SCALE MODEL AND EXPERIMENTAL VALIDATION

MÁRIO PIMENTEL<sup>\*</sup>, AMIN ABRISHAMBAF<sup>†</sup> AND SANDRA NUNES<sup>††</sup>

<sup>\*</sup> University of Porto, Faculty of Engineering  
Porto, Portugal  
e-mail: [mjsp@fe.up.pt](mailto:mjsp@fe.up.pt)

<sup>†</sup> University of Porto, Faculty of Engineering  
Porto, Portugal  
e-mail: [aminab@fe.up.pt](mailto:aminab@fe.up.pt)

<sup>††</sup> University of Porto, Faculty of Engineering  
Porto, Portugal  
e-mail: [snunes@fe.up.pt](mailto:snunes@fe.up.pt)

**Key words:** UHPFRC, tensile response, fibre orientation.

**Abstract:** Ultra-High Performance Fibre-Reinforced cementitious Composites (UHPFRC) designates a family of materials constituted by a compact cementitious matrix reinforced with short high-strength steel fibres. A model is presented based on a meso-level description of the involved mechanics for simulating the direction-dependent tensile response of the UHPFRC. The determination of the relevant material properties and model parameters is discussed. The model is validated with a set of direct tensile tests performed on specimens with varying fibre content and orientation and is shown to be capable of simulating the full tensile responses of both strain-softening and strain-hardening UHPFRCs. Finally, an outlook is given on how the meso-mechanical model can be used to provide the input parameters for the engineering stress-deformation curves describing the anisotropic tensile behaviour of the material and that are suitable for analysis and design of UHPFRC structures.

## 1 INTRODUCTION

The commonly designated Ultra-High Performance Fibre-Reinforced cementitious Composites (UHPFRC) belong to a family of materials constituted by a compact cementitious matrix reinforced with short high-strength steel fibres. This combination provides distinctly high compressive and tensile strengths and excellent durability properties. The material finds application in the rehabilitation and strengthening of existing reinforced concrete structures or in innovative designs of slender structures that can take

advantage of its mechanical properties.

The tensile behaviour of UHPFRC is decisive in many applications and strongly depends on the fibre orientation, which may vary throughout the structure and differ from that of laboratory specimens. Current design practice relies on the use of a scaling factor that can be roughly defined as the ratio between the tensile strength obtained in laboratory specimens and that occurring in the structure. However, it is not only the tensile strength that changes when the fibre orientation varies. In a previous work by the

authors [1] it is shown that the shape of the tensile stress-deformation curve varies significantly, most notably the tensile hardening branch. This is exemplified in Figure 1. Therefore, the influence of the fibre orientation on the tensile behaviour of UHPFRC needs to be investigated and the resulting anisotropic behaviour characterized in order to enable the efficient design of structural UHPFRC elements.

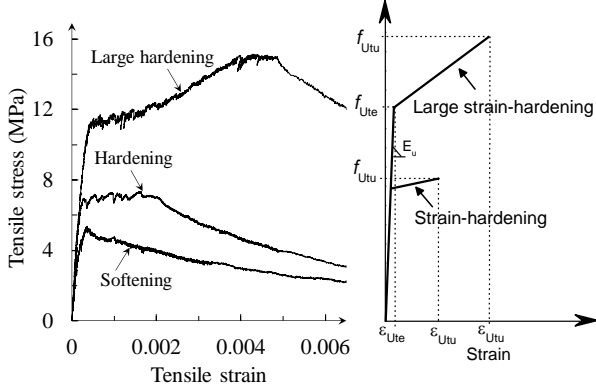


**Figure 1:** Tensile stress-strain curves [1] for UHPFRC with varying fibre content and orientation. Experimental curves (left) and bilinear engineering model (right).

## 2 DESCRIPTION OF THE FIBRE ORIENTATION

As shown in Figure 2, the orientation of a fibre in the 3D space is defined by two angles: the orientation angle,  $\theta$ , and the azimuth,  $\varphi$ . The set of all possible orientations describes a sphere.

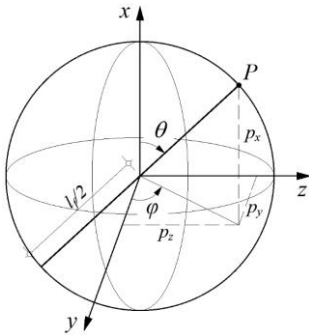


**Figure 2:** Fibre orientation in the 3D space.

The joint probability of a fibre being oriented at  $(\theta, \varphi)$  and crossing the fracture surface normal to the  $i^{th}$  axis is given by Eq. (1), where:  $\psi(\theta, \varphi)$  is the joint probability

density function of fibre orientation;  $p_i(\theta, \varphi)$  is the projection along the  $i^{th}$  axis of the unit vector parallel to the fibre;  $\sin\theta$  comes from the use of spherical coordinates.

$$P(\theta, \varphi) = \psi(\theta, \varphi) p_i(\theta, \varphi) \sin\theta \, d\theta \, d\varphi \quad (1)$$

The function  $\psi(\theta, \varphi)$  is  $\pi$ -periodic. In this work the function proposed by Guenet [2] is adopted:

$$\psi(\theta, \varphi) = K \cdot \cosh[k_g (\cos\theta \cos\theta_0 + \sin\theta \cos\varphi \sin\theta_0)] \quad (2)$$

with

$$K = \frac{k_g}{2\pi \sinh(k_g)} \quad (3)$$

The angle  $\theta_0$  defines the rotation around the z-axis indicating the direction of maximum probability density. The scalar  $k_g$  controls the shape of the function: for  $k_g=0$  the function becomes uniform and for  $k_g \rightarrow \infty$  tends to the Dirac delta function. For intermediate values the function is bell-shaped-

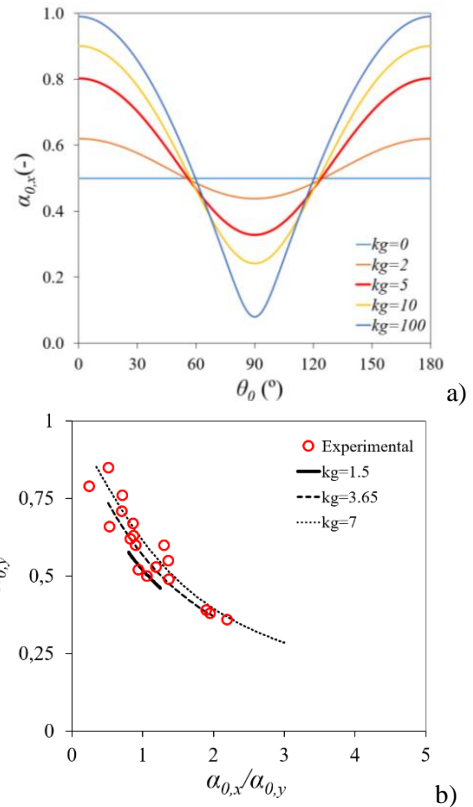


**Figure 3:** Scalar description of the anisotropic fibre orientation using fibre orientation factors.

The fibre orientation factor  $\alpha_{0,i}$  is a scalar descriptor of the fibre orientation that is

proportional to the number of fibres crossing a unit area of the fracture surface normal to the  $i^{\text{th}}$  axis:

$$\alpha_{0,i} = \int_{\varphi_a}^{\varphi_b} \int_{\theta_a}^{\theta_b} \psi(\theta, \varphi) \cdot p_i(\theta, \varphi) \cdot \sin \theta \cdot d\theta \cdot d\varphi \quad (4)$$

The variation of  $\alpha_{0,x}$  with the angle between the fracture surface and the direction of maximum probability density is depicted in Figure 3 a) for varying  $k_g$  values. For uniform fibre distribution ( $k_g=0$ ),  $\alpha_{0,x}=0.50$ , as expected. Increasing  $k_g$  leads to an anisometric distribution of the fibre orientation. The relation between the fibre orientation factors corresponding to two perpendicular directions x- and y- is compared to experimental evidence in Figure 3 b).

The probability density function of the fibre orientation angle,  $\theta$ , of the fibres crossing the surface normal to the  $i^{\text{th}}$  direction is defined by the equation:

$$f_i(\theta) = \frac{1}{\alpha_{0,i}} \int_0^{2\pi} \psi(\theta, \varphi) \cdot p_i(\theta, \varphi) \sin \theta \cdot d\varphi \quad (5)$$

### 3 MODEL FOR THE TENSILE BEHAVIOUR OF UHPFRC

#### 3.1 Concept

The model here presented model is based on the previous works of Pfyl [3], Wuest [4] and Oesterlee [5] and is suited for composites constituted by short steel fibres embedded in a quasi-brittle matrix.

A control volume under uniaxial tension with parallel cracks is assumed. The matrix cracking strength is randomly distributed within the volume. The fibre distribution is described by the joint probability density function  $\psi(\theta, \varphi)$  and by the deterministic fibre volumetric fraction  $V_f$ . The fibre distribution is invariant within the control volume, which is a reasonable assumption if the control volume is small.

The strain hardening response is obtained whenever a stable crack pattern is formed. As in the present model the cracks are subjected to the same stress, a stable crack pattern can only develop if the post-cracking strength

essentially provided by the fibres is larger than the stress required to activate a new crack. The full tensile response of the composite is obtained by performing a force controlled analysis up to the maximum stress and then shifting to crack opening displacement control analysis during the unstable crack propagation stage. In this stage, the deformations are enforced to localize in a single crack, while the others unload. In a uniaxially stressed element with parallel cracks this corresponds to one possible solution to the bifurcation problem occurring at the onset of softening.

Linear elastic behaviour is assumed up to first cracking.

#### 3.2 Behaviour of a single crack

The tensile stress versus crack opening response of each single crack follows the proposal by Li *et al.* [6], considering the additive contribution of the matrix,  $\sigma_{mt}$ , fibre pre-stress,  $\sigma_{pre}$ , and fibre debonding and pullout,  $\sigma_f$  (Figure 4):

$$\sigma_U(w) = \sigma_{mt} + \sigma_{pre} + \sigma_f \quad (6)$$

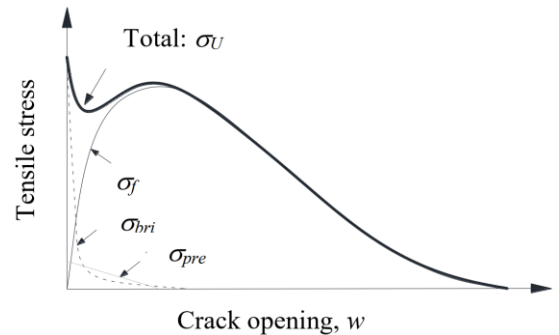


Figure 4: Tensile response of a single crack.

The tensile force transferred by each single fibre intersecting the crack plane is denoted by  $F(l_e, \theta, w)$  and depends on the fibre embedded length,  $l_e$ , on the angle  $\theta$  between the fibre and the normal to the crack surface, and on the crack width,  $w$ . For simplicity, an approximate deconvoluted formulation is adopted:

$$F(l_e, \theta, w) = F(l_e, w)g(\theta) \quad (7)$$

where  $F(l_e, w)$  is the force bridged by an “aligned fibre” and  $g(\theta)$  is the fibre efficiency

function that can be defined as the ratio between the maximum pullout force of a fibre oriented at  $\theta$  and that of an aligned fibre.

The total tensile force transferred by the fibres is obtained by summation of all the fibre contributions, leading to the following equation for  $\sigma_f$ :

$$\sigma_f(w) = \frac{V_f}{A_f} \int_0^{l_f/2} \int_0^{\pi/2} \int_0^{2\pi} F(l_\varepsilon, w) g(\theta) p(l_\varepsilon) P(\theta, \varphi) dl_\varepsilon d\theta d\varphi \quad (8)$$

where  $V_f$  is the volumetric fibre fraction,  $A_f$  is the cross-sectional area of a single fibre,  $P(\theta, \varphi)$  is given by Eq. (1) and  $p(l_\varepsilon)$  is the probability density function of the fibre embedded length. A uniformly distributed embedded length in the domain  $[0; l_f/2]$  is considered, leading to  $p(l_\varepsilon) = 2/l_f$ , with a mean value of  $l_f/4$ .

Defining the fibre efficiency factor,  $\alpha_l$ , as the expected value of the fibre efficiency function of the fibres crossing the fracture surface:

$$\alpha_l = \int_0^{\pi/2} g(\theta) f(\theta) d\theta \quad (9)$$

and considering the definition of  $\alpha_0$  and  $f(\theta)$  given by the Eqs. (4) and (5), Eq. (8) can be re-written as:

$$\sigma_f(w) = \alpha_0 \alpha_l \frac{V_f}{A_f} \int_0^{l_f/2} \frac{2}{l_f} F(l_\varepsilon, w) dl_\varepsilon \quad (10)$$

Pfyl [3] derived an analytical solution for the integral in the right hand side, which is valid if the following simplifications are assumed: (1) rigid-plastic bond stress–slip between the fibres and the matrix; (2) all the fibres undergo simultaneous debonding followed by pullout. (3) the deformability of the matrix is neglected; (4) the elastic deformation of the fibres between the crack lips is disregarded. Under these assumptions, the fibre contribution to the total tensile stress can be obtained in closed form:

$$\sigma_f / f_{Ut,u} = 2 \cdot \sqrt{\frac{w}{w_{deb}}} - \frac{w}{w_{deb}} \quad w \leq w_{deb} \quad (11)$$

$$\sigma_f / f_{Ut,u} = \left[ 1 - 2 \cdot \frac{w}{l_f} \right]^n \quad w > w_{deb}$$

where

$$w_{deb} = (\tau_f l_f^2) / (E_f d_f) \quad (12)$$

marks the onset of the pullout stage. As shown by Pfyl [3], the power  $n$  in the second Eq. (11), describing the descending branch of the curve during the pullout stage that is fully consistent with the assumptions of the model is  $n=2$ . However, other values may need to be adopted to predict the softening stage more accurately. In all the analyses presented in this paper,  $n=4$  is assumed, providing better agreement with the experimental data.

The stress at the peak coincides with post-cracking tensile strength of the composite (recall that the fibre distribution is assumed to be invariant within the control volume) and is given by:

$$f_{Ut,u} = \alpha_0 \alpha_l \frac{l_f}{d_f} V_f \tau_f = \lambda \tau_f \quad (13)$$

which expresses a linear relation between the representative rigid-plastic bond strength,  $\tau_f$ , and the fibre structure parameter,  $\lambda$ . The latter encloses the effects of fibre content ( $V_f$ ), orientation, ( $\alpha_0$ ), efficiency ( $\alpha_l$ ) and shape ( $l_f/d_f$ ), with  $d_f$  being the diameter of circular fibres.

The post-cracking crack bridging stresses transferred by the matrix are modelled using an exponential curve:

$$\sigma_{mt,i} / f_{mt,i} = \exp(-f_{mt,i} \cdot w / G_{Fm}) \quad (14)$$

where  $f_{mt,i}$  is matrix cracking strength corresponding to the  $i^{th}$  crack location and the  $G_{Fm}$  is matrix fracture energy (assumed constant).

The fibre prestress designates the stresses in the fibres due to the elastic deformation prior to cracking. These stresses are assumed to be linearly released after the onset of matrix cracking [7]:

$$\sigma_{pre,i} / f_{mt,i} = \gamma \cdot (w_{deb} - w) / w_{deb} \geq 0 \quad (15)$$

with  $\gamma$  being an homogenization coefficient determined according to Cox [8]. For further details refer to [9].

### 3.3 Simulation of multiple cracking

As proposed by Wuest [4], the random matrix cracking strength is described using a Gaussian distribution. Since the minimum crack spacing must converge to a finite number, two conditions should be simultaneously satisfied to form a new crack: (1) the acting tensile stress should exceed the cracking strength; (2) the distance between two adjacent cracks should be larger than the transfer length:

$$s_{r,\min} = \frac{0.25 f_{mt} d_f}{\alpha_0 \alpha_2 \tau_f V_f} \quad (16)$$

in which,  $\alpha_2 < 1.0$  is a positive scalar accounting for the fact that the fibres are not continuous filaments and are not able to transfer the tensile stresses released by the crack formation stresses so effectively as continuous fibres. Therefore, three parameters are required to simulate the stabilized cracking stage: the mean value of the matrix cracking strength,  $f_{mt}$ , its coefficient of variation,  $CoV$ , and the parameter  $\alpha_2$ . Presently, no spatial correlation is introduced in the model.

## 4 DETERMINATION OF THE INPUT DATA

Table 1 summarizes the required input data, as well as the expected range of values. The data can be divided in three groups: material properties, model parameters and fibre structure parameters.

The required material properties can be determined using well-known experimental methods. The exception is  $\tau_f$ . Although many experimental works involving fibre-pullout tests can be found in the literature, most of the tests refer to fibres aligned at  $0^\circ$  with an embedment length  $l_e = l_f/2$ . However, neither of these two quantities is representative of the fibres crossing a crack in a fibre reinforced composite. Stereology shows that the probability of finding a fibre oriented at  $0^\circ$  with the fracture surface is null. Figure 5 shows the normalized pullout work of smooth fibres with varying orientation. The values are normalized by the pullout work of the fibres at

$30^\circ$  and with the corresponding embedment length. It can be seen that the pullout work of fibres oriented at  $0^\circ$  is much lower than that of the fibres at a small orientation angle.

Moreover, shorter fibres show higher average bond strength than longer fibres of the same type, as evidenced in Figure 6. The average bond strength in a pullout test is given by:

$$\tau_{av} = \frac{P_{\max}}{\pi d_f l_e} \quad (17)$$

with  $P_{\max}$  being the maximum pullout force. This occurs even in straight smooth fibres due to the wedging effect caused by the flattening of the fibre-ends that is formed during the cutting process [9].

**Table 1:** Inpu data

Type	Name		Range of values
Material properties	$E_f$	Steel fibre $E$ -modulus	210 (GPa)
	$E_m$	Matrix $E$ -modulus	40-65 (GPa)
	$G_{fm}$	Matrix fracture energy	0.01-0.035 (N/mm)
	$\tau_f$	Fibre-to-matrix bond strength	6-15 (MPa) – Straight fibres
Model parameters	$f_{mt}$	Mean value of the matrix cracking strength (assuming Normal dist.)	$f_{mt}/\tau_f$ in the range 0.8-1.2
	$CoV$	Coef. of variation of the matrix cracking strength	0.08-0.15
	$\alpha_2$	Crack spacing parameter	0.35-0.45
Fibre structure parameters.	$\alpha_0$	Fibre orientation factor	0.3-0.8(*)
	$\alpha_1$	Fibre efficiency factor	0.50-1.0(*)
	$V_f$	Fibre volumetric fraction	0.015-0.040
	$l_f$	Fibre length	6-30 (mm)
	$d_f$	Fibre diameter	0.15-0.3 (mm)

(\*) The theoretical range is between 0 and 1.0.

Therefore, it is proposed that the representative value of the bond strength to be used in the model is determined from pullout tests on fibres with an embedded length  $l_e = l_f/4$  (which is the average embedded length of the

fibres crossing a crack), and a small inclination angle in the range of  $15^\circ$  to  $30^\circ$ .

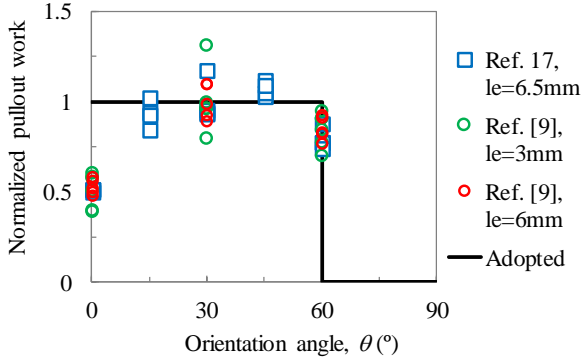


**Figure 5:** Normalized pullout work of smooth fibres.

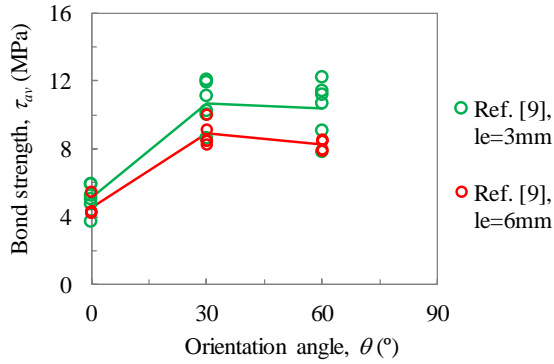


**Figure 6:** Average bond strength of smooth fibres ( $d_f=0.175\text{mm}$ ) [9].

Concerning the fibre structure parameters,  $\alpha_0$  and  $V_f$  are either specified, or can be measured using either destructive (e.g. image analysis of polished surfaces) or non-destructive methods, such as the inductive method described in references [10,11]. As for  $\alpha_1$ , it depends both on the fibre orientation distribution and on the fibre efficiency function  $g(\theta)$ , see Eq. (9). It has been proposed [1,9,11,12,13] to use  $g(\theta)=1$  for  $\theta < 60^\circ$  and 0 otherwise. This is a reasonable proposal provided that the reference bond strength of the “aligned fibres” is based on the results of pullout tests on fibres with a small inclination angle, as discussed above and shown in Figure 5. As proposed by Bastien-Masse *et al.* [14], Figure 7 shows that it is possible to determine  $\alpha_1$  as a function of  $\alpha_0$ . The dots correspond to experimental data obtained from fibre orientation histograms coming from the image

analysis of polished surfaces [1,11,15]. The black lines were determined using Eqs. (9), (5) and (2) for different values of  $k_g$ . The trend observed in the experimental data is well reproduced. The grey line is an empirical equation derived in reference [11] and which can be used to determine  $\alpha_1$  directly from the assumed (or measured) value of  $\alpha_0$ .

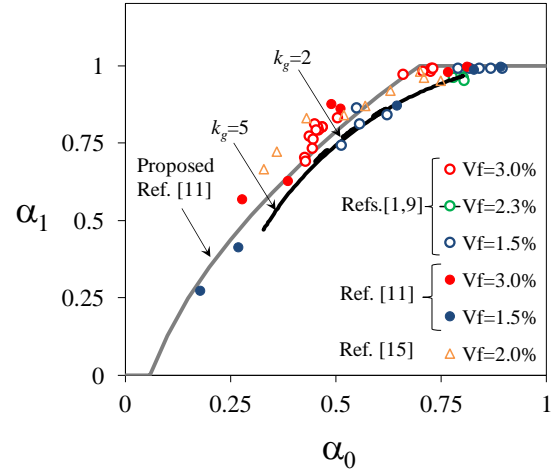


**Figure 7:** Relation between the fibre orientation factor,  $\alpha_0$ , and the fibre efficiency factor,  $\alpha_1$ .

Regarding the model parameters, the values recommended in Table 1 take into account the results of a parametric study developed in reference [9].

## 5 VALIDATION

The model has been validated with experimental data from direct tensile tests on specimens with varying fibre content and orientation. The test specimens had a cross/section of  $30 \times 40 \text{mm}^2$  and were tested with fixed end boundary conditions. The deformations were measured over a base length of 134mm. Polished surfaces of all the specimens were analysed in an image analysis software to obtain the fibre orientation histogram, and the values of  $\alpha_0$  and  $\alpha_1$ . Details can be found in reference [1].

All the simulations were performed with the following input data:  $E_f=210\text{GPa}$ ,  $E_m=40\text{GPa}$ ,  $G_{fm}=0.02\text{N/mm}$ ,  $\tau_f=11\text{MPa}$ ,  $f_{mi}/\tau_f=1.0$ ,  $CoV=0.14$  and  $\alpha_2=0.35$ . Smooth straight  $d_f=0.175$  and  $l_f=9$  and  $12\text{mm}$  (50% of each) were adopted. The stress/strain curves in

Figure 8 corresponding the simulation results (thick black lines) were calculated using the average  $\alpha_0$  and  $\alpha_1$  values corresponding to each orientation profile (not-orient. or well-orient.) and volumetric fibre fraction. The following values were used:

- $V_f=3.0\%$ , well-orient,  $\alpha_0=0.71$ ,  $\alpha_1=0.98$
- $V_f=3.0\%$ , not-orient,  $\alpha_0=0.48$ ,  $\alpha_1=0.80$
- $V_f=1.5\%$ , well-orient,  $\alpha_0=0.84$ ,  $\alpha_1=1.00$
- $V_f=1.5\%$ , not-orient,  $\alpha_0=0.56$ ,  $\alpha_1=0.81$

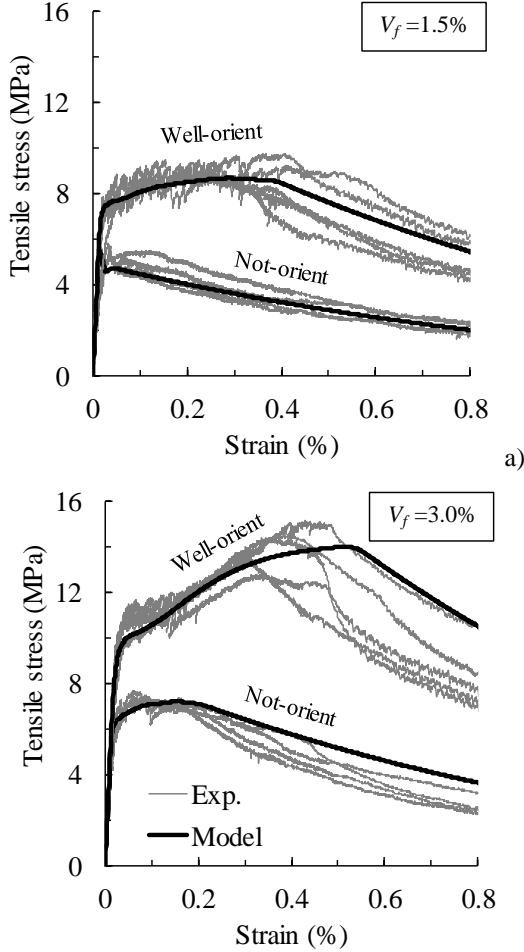


**Figure 8:** Tensile response of the UHPFRC.

The model can be used to obtain the values of  $f_{Ute}$  (conventional limit of elasticity),  $f_{Utu}$  (post-cracking tensile strength) and  $\varepsilon_{Utu}$  (strain at the onset of crack localization) defining the bilinear stress-strain curve for structural or sectional analyses of UHPFRC elements. The results in Figure 9 show that these parameters show excellent correlation with the fibre structure parameter,  $\lambda$ , which confirms the

model assumptions.

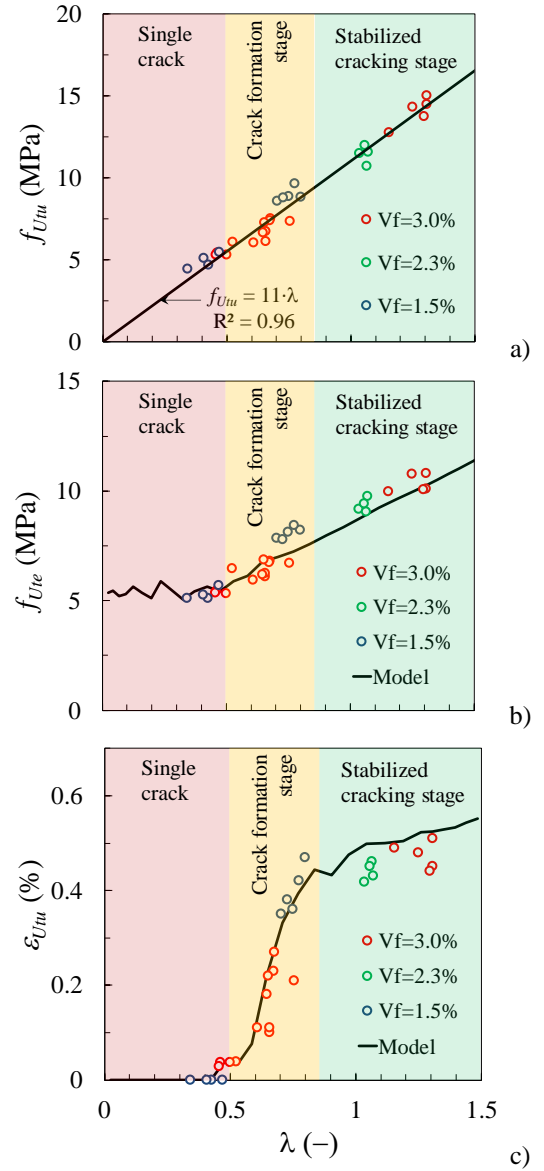


**Figure 9:** Model validation.

The fit exhibited in Figure 9 a) confirms the validity of Eq. (13), which has been previously proposed by Naaman [16] in a similar form. In fact, being the experimental data available, the slope of such line provides the best estimate of representative value of  $\tau_f$  for a particular UHPFRC. However, it must be stressed that one should not expect  $f_{Utu}$  to grow indefinitely with  $\lambda$ . Detrimental fibre grouping effects should start being preponderant above a fibre content threshold and Eq. (13) ceases to be valid. These effects were not observed in the studied UHPFRC up to fibre contents of 3% in

volume.

The plot in Figure 9 c) allows identifying three distinct regimes of tensile behaviour. For the analysed UHPFRC mix, values of  $\lambda < 0.5$  lead to a tensile response without hardening in direct tension. For  $0.5 \leq \lambda < 0.85$  the material exhibits strain hardening in direct tension but the post-cracking tensile strength is reached during the crack formation stage. Small increments of load lead to the formation of more cracks, and therefore  $\varepsilon_{Utu}$  varies sharply with  $\lambda$ . In the case of the tested UHPFRC, this range of  $\lambda$  is the most probable to be found in a real structure where the fibre orientation has been avoided through suitable casting procedures. Therefore, large scatter in the  $\varepsilon_{Utu}$  values is foreseen, since a small variation of the local fibre content/orientation leads to a large variation in  $\varepsilon_{Utu}$ . For  $\lambda \geq 0.85$  the tensile strength is reached during the stabilized cracking stage. In this case, nearly no more cracks are formed upon further load increments, leading to a stagnation of the  $\varepsilon_{Utu}$  value.

## 6 ANISOTROPIC TENSILE RESPONSE

Using the description of the anisometric fibre distribution described in section 2, the model can be used to describe the anisotropic tensile behaviour of the UHPFRC. In Figure 10a) a polar plot is shown with the directional variation of the fibre orientation factor for three fibre orientation distributions corresponding to  $k_g=0$  (isometric), 2 and 5. The last two show preferential orientation of the fibres. For  $k_g=5$  the orientation is quite strong, and hardly achievable only with flow-induced fibre orientation. In Figure 10 b) shows the directional variation of the post-cracking tensile strength of the composite. The calculation of the fibre efficiency factor,  $\alpha_1$ , was made using Eqs. (9), (5) and (2). In Figure 10 c) shows the directional variation of strain at the onset of crack localization,  $\varepsilon_{Utu}$ . It can be seen that the anisotropy is much stronger in the strain than in the stress.

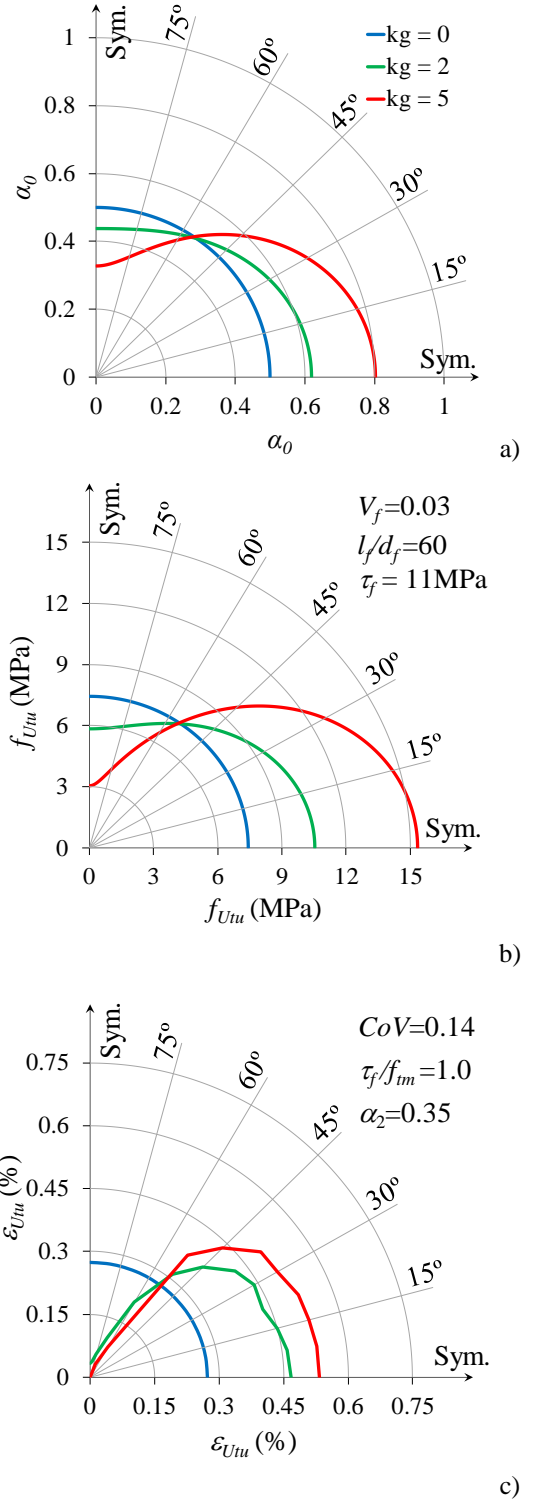


**Figure 10:** Polar plots describing in-plane anisotropic behaviour of the UHPFRC for three fibre orientation profiles corresponding to  $k_g=0, 2$  and  $5$ : a) post peak tensile strength; b) conventional limit of elasticity; c) strain at onset of crack localization.

The step forward is now the development of a constitutive model for structural analysis that is able to incorporate the behaviour described

above. The results in Figure 9 suggest the use of the simple surrogate models proposed in Figure 11. For a particular UHPFRC mix, these models can be calibrated with the results of the meso-mechanical model described in section 3 to provide the directionally dependent values of  $f_{Ute}$ ,  $f_{Utu}$  and  $\varepsilon_{Utu}$  as a function of the directional variation of the fibre structure parameter,  $\lambda$ .

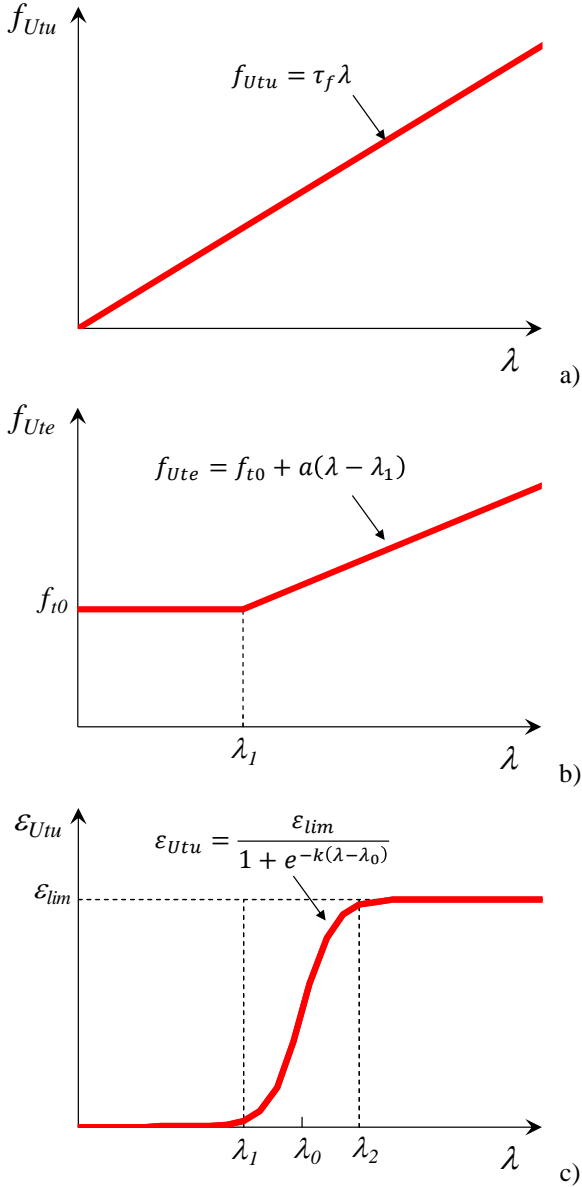


**Figure 11:** Surrogate models for  $f_{Utu}$ ,  $f_{Ute}$  and  $\varepsilon_{Utu}$  as a function of the fibre structure parameter,  $\lambda$ .

## 7 CONCLUSIONS

A mechanical model based on a mesoscale description of the involved mechanics was

presented for describing the direct tensile response of ultra-high performance fibre reinforced cementitious composites. The model was validated with results of direct tensile tests on specimens with a wide range of fibre content and orientation profiles. More important that fitting the experimental results, is the dependency predicted by the model, and confirmed by the tests, between the fibre structure parameter,  $\lambda$ , and the parameters defining the pre-peak tensile response of the composite:  $f_{Ute}$ ,  $f_{Utu}$  and  $\varepsilon_{Utu}$ . This allowed the formulation of simple surrogate models capturing observed (and modelled) trends.

The description of the fibre orientation described in section 2 provides the data necessary to obtain the anisotropic tensile response of the composite, either using directly the meso-mechanical model or the surrogate models. These models should now be extended to include the post-peak part of the tensile response.

Further improvements can be made to the meso-mechanical, most notably the introduction of spatial correlation into the distribution of the matrix cracking strength. Experimental evidence is required to study the detrimental effects of fibre grouping whenever the fibre contents exceed a given threshold.

## 8 ACKNOWLEDGEMENTS

This work was financially supported by: UID/ECI/04708/2019- CONSTRUCT – Instituto de I&D em Estruturas e Construções funded by national funds through the FCT/MCTES (PIDDAC); and by the project POCI-01-0145-FEDER-031777 (UHPGRADE) funded by FEDER through COMPETE2020 - Programa Operacional Competitividade e Internacionalização (POCI) and by national funds (PIDDAC) through FCT/MCTES. Collaboration and materials supply by Concremat, Secil, Omya Comital, Sika, MC-Bauchemie and KrampeHarex is gratefully acknowledged.

## REFERENCES

- [1] Abrishambaf, A., Pimentel, M. and Nunes, S. 2017. Influence of fibre

- orientation on the tensile behaviour of ultra-high performance fibre reinforced cementitious composites. *Cement and Concrete Research*, **97**:28-40.
- [2] Guenet, T., 2016. *Modélisation du comportement des bétons fibrés à ultra-hautes performances par la micromécanique : effet de l'orientation des fibres à l'échelle de la structure*. Doctoral Thesis, Université Paris-Est.
- [3] Pfyl, T., 2003. *Tragverhalten von Stahl-faserbeton*. Doctoral thesis, ETH Zurich.
- [4] Wuest, J., 2007. *Comportement structural des bétons de fibres ultra performants en traction dans les éléments composites*. Doctoral thesis, École Polytechnique Fédérale de Lausanne (EPFL).
- [5] Oesterlee, C., 2010. *Structural Response of Reinforced UHPFRC and RC Composite Members*. Doctoral thesis, École Polytechnique Fédérale de Lausanne (EPFL).
- [6] Li, V.C., Stang, H., Krenchel, H., 1993. Micromechanics of crack bridging in fibre-reinforced concrete. *Materials and Structures*, **26**:486-94
- [7] Li, V.C., Leung, C.K.Y., 1992. Steady-State and Multiple Cracking of Short Random Fiber Composites. *ASCE Journal of Engineering Mechanics*; **188**:2246-64.
- [8] Cox, H.L., 1952. The elasticity and strength of paper and other fibrous materials. *British Journal of Applied Physics*, **3**:72-9.
- [9] Abrishambaf, A., Pimentel, M., Nunes, S., 2019. A meso-mechanical model to simulate the tensile behaviour of Ultra-High Performance Fibre-Reinforced Cementitious Composites. *Composite Structures* (Accepted for publication).
- [10] Nunes, S., Pimentel, M., Carvalho, A., 2016. Non-destructive assessment of fibre content and orientation in UHPFRC layers based on a magnetic method. *Cement and Concrete Composites*, **72**:66-79.
- [11] Nunes, S., Pimentel, M., Ribeiro, F., Milheiro-Oliveira, P., 2017. Estimation of the tensile strength of UHPFRC layers based on non-destructive assessment of the fibre content and orientation. *Cement and Concrete Composites*, **83**:222-38.
- [12] Foster, S. J., 2001. On Behavior of High-Strength Concrete Columns : Cover Spalling, Steel Fibers, and Ductility. *ACI Structural Journal*, **98**:583-9.
- [13] Jungwirth J., 2006 *Zum Tragverhalten von zugbeanspruchten Bauteilen aus Ultra-Hochleistungs-Faserbeton*. Doctoral thesis, École Polytechnique Fédérale de Lausanne (EPFL).
- [14] Bastien-Masse M, Denarié E, Brühwiler E., 2016. Effect of fiber orientation on the in-plane tensile response of UHPFRC reinforcement layers. *Cement and Concrete Composites*, **67**:111-25.
- [15] Duque, L., Graybeal B., 2017. Fibre orientation distribution and tensile mechanical response in UHPFRC. *Materials and Structures*, **50**:1-17.
- [16] Naaman, A. E., 2008. High performance fiber reinforced cement composites. In: Shi C, Mo YL, editors. *High-performance construction materials: Science and applications*. 91-153.
- [17] Lee, Y., Kang, S.T., Kim, J.K., 2010. Pullout behavior of inclined steel fiber in an ultra-high strength cementitious matrix. *Construction and Building Materials*, **24**:2030-41.